POLITECNICO DI TORINO
Repository ISTITUZIONALE

An electrochemical compatibility investigation of RTIL-based electrolytes with Si-based anodes for advanced Li-ion batteries

Original
An electrochemical compatibility investigation of RTIL-based electrolytes with Si-based anodes for advanced Li-ion batteries / Falco, M., Lingua, G., Destro, M., Silvestri, L., Meligrana, G., Lin, R., Fantini, S., Maresca, G., Paolone, A., Brutti, S., Appetecchi, G.B., Elia, G.A., Gerbaldi, C.. - In: MATERIALS TODAY SUSTAINABILITY. - ISSN 2589-2347. - ELETTRONICO. - 21:(2023), p. 100299. [10.1016/j.mtsust.2022.100299]

Availability:
This version is available at: 11583/2974603 since: 2023-01-23T12:48:28Z

Publisher:
Elsevier

Published
DOI:10.1016/j.mtsust.2022.100299

Terms of use:

This article is made available under terms and conditions as specified in the corresponding bibliographic description in the repository

Publisher copyright

(Article begins on next page)

10 September 2026

Materials Today Sustainability 21 (2023) 100299

Contents lists available at ScienceDirect

Materials Today Sustainability

journal homepage: https://www.journals.elsevier.com/materials-today-sustainability

An electrochemical compatibility investigation of RTIL-based electrolytes with Si-based anodes for advanced Li-ion batteries

M. Falco [a, b, *], G. Lingua [a, b], M. Destro [a, b, h], L. Silvestri [c], G. Meligrana [a, b], R. Lin [d], S. Fantini [d], G. Maresca [e], A. Paolone [f], S. Brutti [f, g], G.B. Appetecchi [e], G.A. Elia [a, b], C. Gerbaldi [a, b, **]

[a] GAME Lab, Department of Applied Science and Technology (DISAT), Politecnico di Torino, Corso Duca Degli Abruzzi 24, 10129, Torino, Italy
[b] National Reference Center for Electrochemical Energy Storage (GISEL) - INSTM, Via G. Giusti 9, 50121, Firenze, Italy
[c] ENEA C.R. Casaccia, Energy Department, Via Anguillarese 301, 00123 Roma, Italy
[d] Solvionic SA, Site Bioparc Sanofi, 195 Route D'Espagne BP1169, 31036, Toulouse Cedex 1, France
[e] ENEA, Materials and Physicochemical Processes Technical Unit (SSPT-PROMAS-MATPRO), Via Anguillarese 301, 00123, Roma, Italy
[f] Consiglio Nazionale Delle Ricerche, Istituto Dei Sistemi Complessi (CNR-ISC), Piazzale Aldo Moro 5, 00185, Rome, Italy
[g] Sapienza University of Rome, Department of Chemistry, Piazzale Aldo Moro 5, 00185, Rome, Italy

ARTICLE INFO

Article history:
Received 19 November 2022
Received in revised form
13 December 2022
Accepted 19 December 2022
Available online 26 December 2022

Keywords:
Ionic liquid
Safe electrolyte
Silicon anode
High voltage cathode
Lithium battery

ABSTRACT

Silicon is amongst the most attractive anode materials for Li-ion batteries because of its high gravimetric and volumetric capacities; importantly, it is also abundant and cheap, thus sustainable. For a widespread practical deployment of Si-based electrodes, research efforts must focus on significant breakthroughs to addressing the major challenges related to their poor cycling stability. In this work, we focus on the electrolyte-electrode relationships to support the scientific community with a systematic overview of Si-based cell design strategies reporting a thorough electrochemical study of different room temperature ionic liquid (RTIL)-based electrolytes, which contain either lithium bis(fluorosulfonyl)imide (LiFSI) or lithium bis(trifluoromethylsulfonyl)imide (LiTFSI). Their galvanostatic cycling performances with mixed silicon/graphite/few-layer graphene electrodes are evaluated, with first cycle Coulombic efficiency approaching 90% and areal capacity ≈2 mAh/cm^2 in the limited cut-off range of 0.1−2 V vs. Li^+/Li^0. The investigation evidences the superior characteristics of the FSI-based RTILs with respect to the TFSI-based one, which is mostly associated with the superior SEI forming ability of FSI-based systems, even without the use of specific additives. In particular, the LiFSI-EMIFSI electrolyte composition shows the best performance in both Li-half cells and Li-ion cells in which the Si-based electrodes are coupled with 4V-class composite NMC-based cathodes.

© 2022 The Author(s). Published by Elsevier Ltd. This is an open access article under the CC BY-NC-ND license (http://creativecommons.org/licenses/by-nc-nd/4.0/).

1. Introduction

A new generation of high energy lithium-ion batteries (LIBs) with improved characteristics such as cycling stability, safety and enhanced energy/power density is required to guarantee the massive market deployment of high-demanding applications, which chiefly include electric transportation (EVs, BEVs and PHEVs) and energy storage from renewable power sources [1,2].

The output performance of secondary batteries is necessarily linked to the cell chemistry involved and, so far, LIBs are the only proven commercial technology where stable storage at high energy density is achieved for thousands of reversible cycles [3,4]. Anode materials with high practical capacity as compared to standard commercial graphite (theoretical specific capacity limited to 372 mAh/g) are critical for the purpose, as well as highly ionic conducting, safe and electrochemically stable electrolytes (standard carbonate-based liquid electrolytes are toxic, and their flash point, well below 100 °C, poses significant safety issues) [5]. In this context, silicon (Si) is the most desirable LIB anode candidate due to its high theoretical capacity (even exceeding 4000 mAh/g for

* Corresponding author.
** Corresponding author.
E-mail addresses: marisa.falco@polito.it (M. Falco), claudio.gerbaldi@polito.it (C. Gerbaldi).
[h] Now at Battery Global Competence Center, Comau S.p.A. – Electrification, Via Rivalta 49, 10095 Grugliasco (TO), Italy.

https://doi.org/10.1016/j.mtsust.2022.100299
2589-2347/© 2022 The Author(s). Published by Elsevier Ltd. This is an open access article under the CC BY-NC-ND license (http://creativecommons.org/licenses/by-nc-nd/4.0/).

$Li_{22}Si_5$, which is the highest known value for a LIB anode material), average de-lithiation potential of about 0.3–0.4 V vs. Li^+/Li^0, which likely avoids lithium dendrite formation during charge, high abundancy reserves (about 28%, the second most abundant element in the Earth's crust, being surpassed only by oxygen) and relatively low cost (much lower in terms of US$/Kg compared to lithium metal and slightly lower even compared to pure natural graphite, which is also included in the 2020 EU list of Critical Raw Materials – CRM) [6–8]. However, Si undergoes significant volume variations upon lithium alloying/dealloying (up to ≈ 400%), resulting in dynamic (unstable) interface formation and, eventually, anode pulverisation upon prolonged cycling, which breaks the electrical contact within the active material particles as well as with the current collector. This phenomenon may lead to the continuous disruption, propagation and thickening of the solid electrolyte interphase (SEI) layer, which gives rise to undesirable side reactions with the electrolyte, resulting in its dynamic consumption/reformation during operation and, in turn, rapid deterioration of cell capacity and operational life. In addition, Aurbach and coworkers previously reported that Si has a poor electronic conductivity in its delithiated form (1 mS/cm) [9] and the lithium diffusion coefficient in the material structure is low (10^{-14}–10^{-13} cm^2/s) [6–8,10].

To circumvent these issues and enhance stable and reversible lithium storage performances, Si-based materials and silicon-carbon (Si–C) composites with different dimensionality from micro/nanoparticles to 3D architectures were proposed [8,10,11]. These include various nanostructure designs (e.g., nanoparticles, nanowires, nanotubes/pillars, nanoflakes, and nanoporous films), often combined, dispersed or enwrapped in various carbonaceous matrices, either graphitic or amorphous and even porous. More recently, several works were proposed, which included graphene (G) in its different forms (e.g., graphene oxide – GO and reduced graphene oxide – RGO, and few-layer graphene – FLG flakes) [12–15]. Despite these strategies being useful to buffer Si volume variations and increase the anode conductivity, the increased surface area amplifies the issues related to the interfacial reactions with the electrolyte upon cycling, due to the aforementioned recurring disruption/formation of the SEI layer [8,16]. One of the most practised routes to stabilise the SEI layer consists in the use of functional additives, such as vinylene carbonate (VC), fluoroethylene carbonate (FEC), silanes, compounds bearing nitrogen-containing functional groups, such as nitrile and isocyanate moieties, and boron-containing lithium salts [16,17].

Electrolytes based on room temperature ionic liquids (RTILs) have been widely investigated and proven to be a viable alternative enabling reversible operation of laboratory-scale cells with Si-based anodes for hundreds of cycles, outperforming in many cases the liquid electrolytes based on standard organic carbonates [18–21]. Additionally, RTILs possess several superior properties in terms of safety (low vapour pressure and flame retarding ability) and stability, both thermal and electrochemical [22–25], which are highly attractive for practical operation in the EV battery market [1]. RTILs with phosphonium-, pyrrolidinium-, piperidinium-, and imidazolium-based cations were investigated in combination with Si-based anodes [1,2,17–19,26–28]. Notably, both the rate and long-term cycling performances were found to be drastically affected by the anion, when a direct comparison was provided. In particular, systems with bis(fluorosulfonyl) imide (FSI^-) showed a neat improvement over the bis(trifluoromethansulfonyl) imide ($TFSI^-$) counterparts due to their lower interfacial resistance, better transport properties and SEI-forming ability, which can also prevent the detrimental co-intercalation of RTIL cations into graphite [1,2,17–19,27–30]. Nevertheless, FSI-based systems show a lower decomposition temperature (T_d) as compared to their TFSI counterparts, particularly LiFSI, for which T_d is also affected by adsorbed water and impurities, and can vary from 70 to 180 °C (whereas T_d > 380 °C for LiTFSI) [30–33]. Therefore, mixed RTIL-based systems are desirable, including both FSI^- and $TFSI^-$ anions, and such systems already demonstrated the ability to tune the electrolyte properties for improving cell performance [20,21,34]. Electrolytes with a Li^+ salt:RTIL molar ratio of 1:4 were proven particularly promising [35,36].

In the framework of the H2020 European (EU) project Si-DRIVE (https://sidrive2020.eu/), we are now focusing our research on developing novel optimised materials to achieve high energy density, long-term operation LIBs able to meet the present challenges of EVs and related EU market opportunities. Si-DRIVE is intended to deliver on the challenge of safer, higher-performing LIB chemistries for future EVs by the integrative development of full cells that can deliver high energy density (>350 Wh/kg at 6C and >1000 primary cycles by the end of the project) by exploiting a nanostructured Si-based active material anode, a high-capacity Li-rich layered oxide cathode and a safe, highly ionically conducting RTIL-based electrolyte. In this context, electrodes based on silicon and FLG obtained by a wet jet-milling process are investigated in this work. Similar binder-free Si-FLG electrodes have already demonstrated excellent performances in lab-scale cells, with a specific capacity ≈2300 mAh/g_{Si}, and only 11% irreversible capacity loss during the first cycle using a carbonate ester-based electrolyte [37,38]. Yet, with a RTIL-based electrolyte containing $TFSI^-$, reversible cycling of Si-FLG could only be observed at 80 °C, with significantly lower specific capacity (<800 mAh/g_{Si}) [39]. In contrast, promising results with TFSI-based RTIL electrolytes in combination with several different silicon-based anodes have been reported, implying the need to select the electrolyte depending on the electrode composition and morphology [17]. Therefore, starting from the significant amount of work regarding different Si-based anodes in combination with RTIL based electrolytes [18,40,41], we performed and assessed various RTILs with different cations and anions. Specifically, here we address the compatibility with the Si-FLG electrode material used in this work, which is also distinguished by the cycling protocol adopted (e.g. lower voltage cut-off of 0.1 V vs Li^+/Li^0) to limit Si volume variations and exclude the contribution of the carbon material to the delivered capacity. In this respect, the reported electrochemical investigation revealed the superior performance of the Si-FLG-based electrodes in combination with RTIL-based electrolytes, compared with organic solvent-based electrolytes. Additionally, systems including FSI and TFSI are investigated, evidencing differences in the electrochemical performance depending on the cathode loading and the RTIL cation.

Thus, as a result of the screening performed in the framework of Si-DRIVE project, here we report a comparative investigation of the most promising electrolyte compositions, which include RTILs containing FSI^- anion and 1-ethyl-3-methyl imidazolium (EMI^+) or pyrrolidium-based ($Pyr^+_{1,R}$) cations, added with either LiFSI or LiTFSI, to allow stable cycling of nanostructured Si-based anodes at high performance, an utmost important topic in the LIB field [18,37–40]. The effect of the different RTILs, lithium salts and additives, such as VC and FEC, on the electrochemical performance of Si-based electrodes, was evaluated in lab-scale lithium metal cells and discussed. Selected electrolytes then underwent constant-current testing in lab-scale Li-ion cells, where Si-based anodes were coupled with NMC-based cathodes, which demonstrated reversible cycling at ambient temperature and different current regimes up to 1C rate, thus confirming their promising prospects for practical application.

2. Experimental

2.1. Materials

The different RTILs (>99.9 wt%, moisture content <5 ppm), including 1-ethyl-3-methyl-imidazolium bis(fluorosulfonyl)imide

(EMIFSI), N-methyl-N-propyl-pyrrolidinium bis(fluorosulfonyl) imide ($PYR_{13}FSI$) and 1-methyl-1-(2-methoxyethyl)pyrrolidinium bis(fluorosulfonyl)imide ($PYR_{1(2O1)}FSI$), the lithium salts (>99.9 wt %, moisture content <5 ppm), including lithium bis(fluorosulfonyl) imide (LiFSI) and lithium bis(trifluoromethanesulfonyl)imide (LiTFSI), and battery-grade additives (i.e., fluoroethylene carbonate − FEC, and vinylene carbonate - VC) were synthesized by *Solvionic* (Toulouse, France) and used as received.

Commercial silicon micron-sized particles (*Silgrain,* e-Si 400 from *Elkem*), carbon additives (Super C-45 and C-65 from *Imerys*, formerly *Timcal*), NMC 532 ($LiNi_{0.5}Mn_{0.3}Co_{0.2}$, *BASF*), polyvinylidene fluoride (PVdF, Solef 5130 from *Solvay*), and few-layer graphene flakes obtained by a wet jet-milling process [42] were used as received. Lithium hydroxide ($LiOH{\cdot}H_2O$), polyacrylic acid (PAA), and N-methyl pyrrolidone (NMP) were supplied by *Sigma-Aldrich* (now *Merck*).

The battery grade reference electrolyte ($LiPF_6$ 1 M in EC/PC/EMC/DEC + 2 wt% VC) was provided by Capchem and used as received.

2.2. Preparation and characterisation of the RTIL-based electrolytes

The RTIL-based electrolyte formulations were prepared within a controlled Ar-atmosphere dry glovebox (*MBraun UNILab*, H_2O and O_2 content <1 ppm): proper amounts of selected lithium salt were dissolved in each RTIL by stirring at ambient laboratory temperature for few hours. The RTIL:lithium salt molar ratio was fixed equal to 4:1 [36]. Additional samples were prepared by adding FEC or VC to each electrolyte solution. The compositions of all electrolyte formulations under study are given in Table 1.

The ion transport properties of the RTIL-based electrolytes were investigated in terms of ionic conductivity (σ) *vs*. temperature dependence. The measurements were carried out in a wide temperature range of −40 to 80 °C at a very slow heating scan rate (<1 °C/h) for better evidencing the phase transitions [22]. A conductivity-meter AMEL 160, allowing to run impedance measurements at a fixed frequency (i.e., 1 Hz or 1 kHz, depending on the conduction value of the sample under test) was used, whereas the temperature control was allowed by a climatic test chamber (Binder GmbH MK53). The electrolytes (handled in the dry glovebox) were housed in sealed glass conductivity cells (AMEL 192/K1) equipped with two porous platinum (Pt) electrodes. The cell constant (i.e., depending on the geometric characteristics of the cell under test) was determined through a 0.1 N KCl aqueous solution with a known ionic conductivity value. To fully crystallise the RTIL electrolytes, the cells were dipped in liquid nitrogen for 60 s and, then, immediately transferred into the climatic chamber (previously set-up at −40 °C). This protocol was repeated until the frozen RTIL samples remained solid at −40 °C. In a previous work, the incomplete crystallisation of RTILs was demonstrated to result in pseudo-equilibrium (metastable) states affecting both their thermal and transport properties [43]. Finally, the cells were kept at −40 °C for at least 24 h before the conductivity measurements.

To confirm the reproducibility of the ion conduction values and for gaining knowledge about phase transition phenomena within the RTIL-based electrolyte formulations, the specific conductivity values were also determined by electrochemical impedance spectroscopy (EIS). During the measurement, an alternating sinusoidal voltage was applied to the electrochemical cell under examination in a given frequency range, with frequency sweep towards progressively decreasing values. At high frequencies, the impedance response is related to fast processes (ion transport in the electrolyte), whereas, at progressively decreasing frequencies, it allows obtaining information on slower processes (charge transfer at the electrolyte/electrode interface, diffusion within the electrolyte and electrode, etc.). In addition, the electrochemical system under examination can be simulated using a circuit model consisting of resistors and/or capacitors (connected in series and/or parallel), which represent the contributes to the overall impedance of the system. Through a proper fitting program, it was possible to separate the contributes to the overall impedance of the investigated electrolyte and, therefore, determine its resistance value. EIS measurements were performed (using a Schlumberger Solartron 1260 frequency response analyser) by applying, to the conductivity cells described above, a sinusoidal voltage signal (ΔV) equal to 10 mV in a frequency range between 100 kHz and 1 Hz. The impedance measurements were conducted in the −40/+80 °C temperature range, and immediately after carrying out the conductometric measurements. The ionic conductivity (σ) was determined through the following relationship (Eq. (1)):

$$\sigma = k/R \tag{1}$$

where k is the cell constant and R represents the (ionic) resistance (determined by EIS) of the RTIL electrolyte under examination.

2.3. Preparation of the Si-based and NMC-based composite electrodes

The Si-based electrode tapes (namely, SiGPAA) were obtained from an aqueous slurry containing 80 wt% of a mixture (1:1 ratio) of Si particles and graphene flakes as the active materials, 10 wt% of C-45 and 10 wt% of LiPAA binder. LiPAA binder was previously

Table 1
Composition and properties of the RTIL-based electrolytes under study.

Electrolyte	RTIL/Li mole ratio	RTIL/Li wt.%	Additive content /wt.%	σ (−10 °C) /(mS/cm)	σ (0 °C) /(mS/cm)	σ (20 °C) /(mS/cm)
EMIFSI						
+ LiFSI	4/1	86.2/13.8	0	2.3 ± 0.2	3.8 ± 0.4	8.4 ± 0.8
+ LiTFSI	4/1	80.2/19.8	0	1.5 ± 0.1	2.6 ± 0.3	6.0 ± 0.6
+ LiTFSI/VC	4/1	77.8/19.2	3	–	–	–
+ LiTFSI/FEC	4/1	77.8/19.2	3	–	–	–
$Pyr_{1(2O1)}FSI$						
+ LiFSI	4/1	87.4/12.6	0	0.65 ± 0.06	1.2 ± 0.1	3.0 ± 0.3
+ LiTFSI	4/1	81.9/18.1	0	0.52 ± 0.03	1.0 ± 0.1	2.7 ± 0.3
+ LiTFSI/VC	4/1	79.4/17.6	3	–	–	–
+ LiTFSI/FEC	4/1	79.4/17.6	3	–	–	–
$Pyr_{13}FSI$						
+ LiFSI	4/1	86.8/13.2	0	1.1 ± 0.1	1.8 ± 0.2	4.3 ± 0.4
+ LiTFSI	4/1	81.1/18.9	0	0.63 ± 0.06	1.1 ± 0.1	3.0 ± 0.3
+ LiTFSI/VC	4/1	78.7/18.3	3	–	–	–
+ LiTFSI/FEC	4/1	78.7/18.3	3	–	–	–

prepared as a 4 wt% aqueous solution of $LiOH \cdot H_2O$ in stoichiometric amount and PAA. The slurry preparation was performed by means of a mechanical mixer equipped with a sparger. First, graphene flakes were added to the binder solution and stirred for 20 min to allow homogeneous particle dispersion. C-45 was then added under slow continuous stirring, followed by a fast mixing step of 10 min. Lastly, the Si particles were slowly added to the slurry, followed by a high shear rate mixing step of 60 min. A final 30 min step of gentle mixing in vacuum was performed to remove any air bubbles. The slurry was deposited onto a 250 mm wide and 10 μm thick Cu current collector foil by means of a semi-automated doctor blade coater, using two different gaps to obtain two different mass loading values (namely, 1.03 ± 0.03 and 2.54 ± 0.04 mg/cm^2). Water was removed by drying the casted electrodes during two consecutive steps (60 min each) at increasing temperatures of 70 and 120 °C, respectively.

The NMC-based composite positive electrodes were obtained from a slurry containing 94 wt% of NMC as the active material, 3 wt % of C-65 as the carbon additive and 3 wt% of PVdF as the binder. PVdF was pre-solubilised in a 10 wt% NMP solution as basis for the slurry preparation. The slurry was deposited onto a 250 mm wide and 20 μm thick Al current collector foil by means of a semi-automated doctor blade coater. The solvent was removed by drying the casted electrode during two consecutive steps (30 min each) at increasing temperatures of 70 and 120 °C. Eventually, the SiGPAA and the NMC electrode tapes were cut into disks, dried at 120 °C under vacuum for 24 h and stored in the Ar-filled dry glovebox before their assembly and testing in lab-scale test cells.

2.4. Assembly of laboratory-scale Li-metal and Li-ion cells and electrochemical testing

The Li-metal cells for the electrolytes comparison were assembled by sandwiching the components in a Li/electrolyte/SiGPAA configuration, with lithium metal (*Albemarle*) counter and SiGPAA (with a mass loading of 2.54 ± 0.04 mg/cm^2) working electrode disks having an area of 2.01 cm^2. The Li-metal cells for the derivative dq/dV analysis of the first lithiation were assembled with SiGPAA electrodes having a loading of 1.03 ± 0.03 mg/cm^2. The Li-ion cells were assembled in a SiGPAA/electrolyte/NMC configuration, with SiGPAA anodes and NMC cathodes having an area of 2.54 cm^2 and a mass loading of 1.18 ± 0.06 and 7.97 ± 0.06 mg/cm^2, respectively. Two glass fiber (Whatman® GF/A) 100 μm thick disks (2.54 cm^2 area) were used as separators, drenched with 200 μL of selected RTIL-based electrolyte. The above detailed cell assemblies were housed in ECC-Std lab-scale test cells (*EL-Cell Gmbh*), which were used for carrying out the electrochemical testing. The lab-scale cells were assembled inside the dry glovebox and cycled at ambient temperature under constant current (CC) regime with an Arbin BT2000 battery tester. Based on previous work evaluations [38], the maximum practical specific capacity of Si-graphene composites is ≈ 2500 mAh/g$_{Si}$ in the 0.1–1 V vs Li^+/Li^0 range. Here, for the Li//SiGPAA cells, we used C-rate values of C/10, C/5, C/2 and 1C, corresponding to 250, 500, 1250, 2500 mA/g$_{Si}$, respectively. The CC cycling was carried out in the cut-off voltage range 0.01–2 V vs Li^+/Li^0 (for the first cycle, to ensure the formation of the SEI and the amorphisation of Si) and 0.1–1 V vs Li^+/Li^0 (for the following cycles), see Fig. S1 in the supporting information. For the SiGPAA//NMC Li-ion cells, the CC cycling test was carried out in the range 4.25–3 V vs Li^+/Li^0, with a constant voltage step at 4.25 V after each CC charge, which was kept until the current reached the value of C/50. The 1st CC charge was carried out at C/10 based on the charge capacity of the NMC used (≈200 mAh/g, *viz.* ≈1.5 mAh/cm^2, see Fig. S2). For the following CC steps, the C-rate was calculated based on the estimated cell capacity, which was obtained by subtracting the irreversible capacity of the anode (computed as the difference between the lithiation and de-lithiation capacity during the 1st cycle in lab-scale Li-metal cells, see Fig. S3 and Table 3) from the charge capacity of the NMC used. The N/P ratio (the ratio between the delithiation capacity of the negative electrode and the discharge capacity of the positive electrode) is also given in Table 3. The discharge capacity of the NMC positive electrode used is ≈ 190 mAh/g, *viz.* ≈1.4 mAh/cm^2 (see Fig. S2).

2.5. ATR-FTIR characterisation of the SEI

ATR-FTIR analysis was performed on *post-mortem* electrodes collected from Li/electrolyte/SiC half-cells after 10 cycles at C/10. Model composite electrodes were manufactured starting from commercial silicon nanoparticles (Sigma Aldrich, <100 nm particle size) added with carbon black and FLG, following a procedure similar to what described in Ref. [44]. Electrodes for ex situ analysis were collected in the following steps: cell de-assembling in an Ar-filled glove box followed by electrode washing in tetrahydrofuran and vacuum drying at room temperature. *Post-mortem* materials have been stored in sealed vials in the Ar-filled glove box. Fast Fourier transform infrared spectra in attenuated total reflectance (ATR-FTIR) were collected at the SMIS beamline of Synchrotron Soleil in air by a Thermo Nicolet 8700 Continuum microscope, equipped with a 15X - Schwarzschild ATR objective, that employs a ZnSe crystal with a refractive index of n = 2.4 (ISP Optics Corp., Latvia). The spectra were recorded in the mid-infrared spectral range (from 400 cm^{-1} to 4000 cm^{-1}) using synchrotron light as source, a KBr beam-splitter and a liquid nitrogen cooled MCT detector. All the reported spectra were obtained by adding up 500 scans, with a spectral resolution of about 2 cm^{-1}.

3. Results and discussion

3.1. Properties of the RTIL-based electrolytes

The electrolyte solutions were prepared as detailed in the experimental section, and their compositions are summarised in Table 1.

The impedance responses obtained for the investigated RTIL-based electrolyte formulations are shown as Nyquist diagrams (real part Z′, vs. imaginary part -jZ″) at different temperatures, as illustrated in Fig. 1 for the electrolyte comprising LiFSI and EMIFSI reported as an example (i.e, all investigated electrolyte formulations have shown analogous qualitative behaviour). At low temperatures (−20 °C, *viz.* below the melting point of the electrolyte), the sample shows the typical impedance response of an electrolyte sandwiched between two blocking electrodes (panel A). The diameter of the high frequency semicircle (100–1 kHz), originating at the point of intersection of the axes, is associated with the ionic resistance of the electrolyte (R_b) [45]. The impedance diagram is only slightly depressed, indicating that the overall resistance of the electrolyte is substantially given by a single contribute [45]. The qualitative shape of the Nyquist diagram changes considerably at temperatures ≥ −15 °C (panel B): the disappearance of the high frequency semicircle is observed with the increase in temperature, due to the decrease of the electrolyte resistance (note that the frequencies of the points of the semicircle fall at frequencies higher than the full scale of the instrument). The distance between the origin of the axes and the high frequency diagram intercept with the Z′ axis is associated with the electrolyte resistance (panel D) [45].

The inflexion recorded at medium-high frequencies suggests the presence of a second contribution (negligible at low temperatures since the R_b value is very high), which, however, cannot be

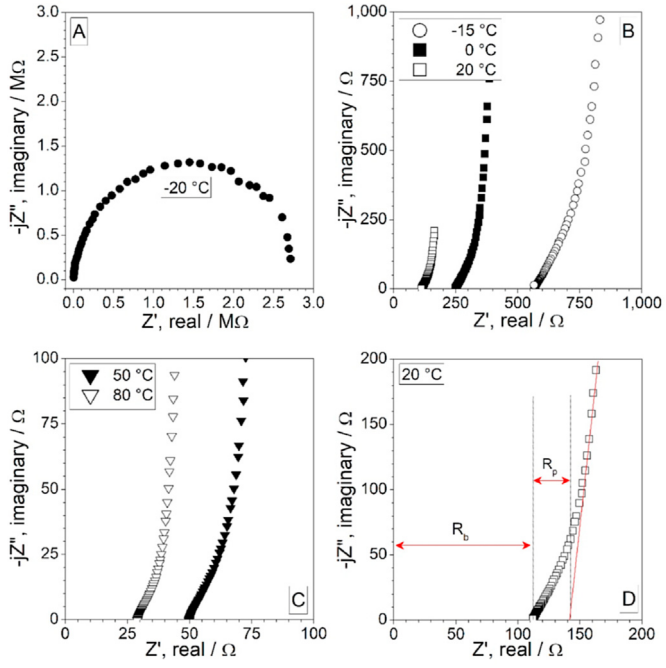

Fig. 1. Representative Nyquist diagrams (Z′ vs. -jZ″) of the impedance responses obtained for the LiFSI-EMIFSI electrolyte in a conductivity cell with porous Pt electrodes at: A) − 20 °C below the melting point; B) different temperatures in the range between the melting point and 20 °C, as noted in the legend; C) different high temperatures as noted in the legend, D) 20 °C, including the fitting lines and the attribution of the spectral features to the bulk resistance (R_b) and resistance due the electrode surface roughness behaving as a porosity (R_p).

attributed to heterogeneous phase since, at −15 °C, the LiFSI-EMIFSI sample is in the liquid state. Furthermore, the value of the capacitance (C_p) associated with the aforementioned contribute is excessively high (of the order of mF) with respect to that related to a geometric and/or grain boundary capacitance [45]. Data reported in the literature [46] show how this capacitance is attributable to the high surface roughness of the electrode, which behaves like a porous surface. Therefore, the effective area of the electrode is significantly amplified, resulting in an increase in terms of capacitance equal to several orders of magnitude with respect to that associated with smooth electrodes. The additional contribute to the overall cell impedance is ascribable to the resistance (R_p) encountered by the ions in crossing the roughness, behaving as a porosity, of the electrode (panel D). Finally, the straight line at lower frequencies (<1 kHz) is due to the capacitive behaviour at the Pt blocking electrode. An increase in temperature above −15 °C (panels B and C) does not produce any change in the shape of the Nyquist diagram and results only in a progressive shift of the high frequency intercept towards lower resistance values ascribable to the decrease of the electrolyte resistance (with the temperature increase).

The analysis of the impedance responses was performed by defining an equivalent circuit model considering all the possible contributions to the impedance of the electrolyte under investigation [47,48]. The validity of the chosen circuit was confirmed by means of a non-linear fitting program (NLLSQ) [47,48]. The goodness of the fitting operation was quantified by the parameter χ^2: only interpolations with $\chi^2 < 10^{-4}$ were considered acceptable. The equivalent circuit (Fig. S4 in supporting information), adapted for the interpolation of Nyquist diagrams obtained up to −20 °C (panel A), consists of the resistance R_b (electrolyte resistance) placed in parallel with the geometric capacitance of the electrolyte (C_g). The R_bC_g circuit net is in series with the double layer capacitance at the electrolyte/electrode interface (C_{dl}) [45]. Conversely, the AC responses obtained at T ≥ −15 °C were fitted with the circuit model shown in panel B, consisting of the resistance R_b placed in series with the R_pC_p (i.e, the additional R_p and C_p elements, with respect to the circuit model A, take into account the roughness of the electrodes) and, subsequently, with the capacitance C_{dl}.

The temperature dependence of the ionic conductivity of the investigated binary electrolytes is shown in Fig. 2. The ion conduction values determined by EIS are very close to those obtained through the conductivity-meter (data not reported). The LiFSI-EMIFSI sample (panel A) shows a jump in the ionic conductivity of about four orders of magnitude, just above −20 °C, related to the melting of the RTIL electrolyte.

Conversely, LiTFSI-EMIFSI exhibits progressively increasing conductivities from −40 °C, indicating a gained ion mobility with a knee around −20 °C. This behaviour, also observed for the $PYR_{1(201)}FSI$ (panel B) and $PYR_{13}FSI$ (panel C) based samples, is likely ascribable to solid-solid phase transition [49] occurring

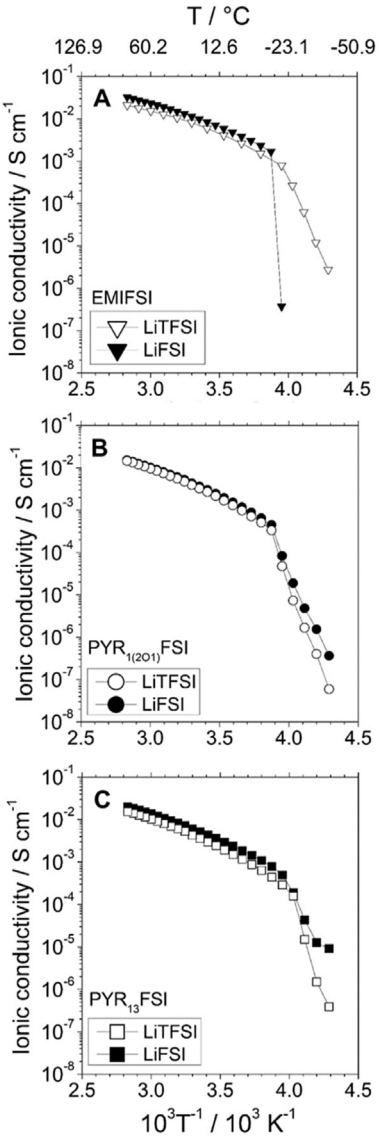

Fig. 2. Arrhenius plot of the ionic conductivity data extracted from the analysis of the electrochemical impedance response of conductivity glass cells with porous Pt electrodes filled with different RTIL-based electrolytes containing LiTFSI or LiFSI as noted in the legend.

within the RTIL electrolytes prior to melting. For instance, ionic conductivities above 10^{-5} S/cm are exhibited already at −30 °C, which is undoubtedly interesting for electrolytes being in the solid-state. Incorporating an oxygen atom into the pyrrolidinium cation increases the melting temperature (indicated by the sudden slope change in the ionic conductivity *vs*. temperature plot). An analogous trend, previously observed for tetra-alkyl-ammonium [36] and imidazolium RTILs [50], is likely ascribable to repulsive interactions of the oxygen electron lone pairs with the neighbouring anions. At temperatures ≥ −15 °C (i.e., above the melting point of the IL electrolytes), all of the samples under study are in the liquid state and show a VTF trend (witnessed by the non-linear trend of the Arrhenius conductivity plots), typical of RTIL electrolytes [22,36], up to 80 °C. EMIFSI-based electrolytes show faster ion transport properties with respect to those based on pyrrolidinium cations. This behaviour was previously reported in the literature [22,36] and might be attributed to the smaller steric hindrance and the planar configuration of the imidazolium cation, which can slide through the ionic medium more easily compared to the pyrrolidinium one. The LiFSI-containing electrolytes provide moderately higher ion conduction due to their lower viscous drag deriving from the smaller steric hindrance of the FSI^- anion if compared to $TFSI^-$. The $PYR_{1(2O1)}FSI$ based electrolytes display a slightly lower ionic conductivity than the $PYR_{13}FSI$ based ones, which is linked to the more significant steric hindrance of the methoxyethyl chain with respect to the n-propylene. The ion conduction values of the investigated RTIL are summarised in Table 1. All the investigated systems show ionic conductivity exceeding 10^{-4} S/cm (or 10^{-3} S/cm) already at −10 °C, i.e., appealing values for application in secondary batteries operating even at low temperatures. In all cases, high ionic conductivity values ranging from 10^{-3} to 10^{-2} S/cm are obtained at ambient temperature (20 °C).

3.2. Electrochemical behaviour in Li-metal cells with Si-based anodes

For the proper selection of a safe electrolyte formulation to be exploited in combination with Si-based anodes, the compatibility and characteristics of the different RTIL-based electrolyte formulations were preliminarily tested, in terms of galvanostatic charge/discharge behaviour, in laboratory-scale Li-metal cells. SiGPAA anode is used as the reference material for the testing [38], characterised by a practical capacity value of ≈2500 mAh/g_{Si} (see Table 2 and Fig. S1), utilising the carbonate-based liquid electrolyte. The SiGPAA electrode delivers a relatively good capacity in the conventional carbonate-based electrolyte; however, the specific capacity at 1C and the capacity retention after the rate capability test are poor (≈100 mAh/g_{Si} and 66%, respectively). It suggests poor quality of the passive layer, which is highly resistive and ineffective in stabilising the electrochemical performance, thus leading to significant capacity fading and the deterioration of the cell performance at high current regimes [18]. The proper selection of the electrolyte can mitigate the limited performance of the Si-based anode; particularly, ILs-based electrolytes are considered extremely promising to guarantee improved performances [1,2,17–19,26–28].

To further investigate this aspect, Li/SiGPAA cells (SiGPAA loading ≈ 1.03 mg/cm^2, i.e. ≈ 0.41 mg_{Si}/cm^2) were assembled and tested by means of galvanostatic cycling at low current (0.047 mA/cm^2, i.e. 115 mA/g_{Si}) with a lower cut-off voltage of 0.01 V (see Fig. S5). Fig. 3 shows the derivative dQ/dV analysis plot for the first lithiation.

In the presence of EMI^+, a peak is clearly visible at ≈ 0.7 V (inset in Fig. 3), indicating an electrochemical process occurring, which is absent in the other cases; it can be attributed to EMI^+ decomposition at the surface of the SiGPAA electrodes. Limiting the SiGPAA electrode loading (≈1.03 mg/cm^2) and the current density (115 mA/g) leads to good cell performance, regardless of the electrolyte composition. Under this condition, the de-lithiation areal capacity delivered in the range 0.01–2 V is up to 2 mAh/cm^2. Operation in the voltage range 0.01–2 V is fundamental to ensure the SEI formation and the amorphisation of Si during the first cycle [51]. However, during the following cycles, the cut-off voltage window can be limited to 0.1–1 V to avoid extreme volume variations of Si upon the lithiation/de-lithiation processes as a trade-off between the delivered specific capacity and the cycling ability [38].

Considering Si-DRIVE project targets, in line with EV application requirements, cells with a practical areal capacity of ≈2.5 mAh/cm^2 in the range of 0.1–1 V (Fig. S1), corresponding to a Si mass loading of ≈1.0 mg/cm^2_{Si} (2.5 mg/cm^2 for the complete electrode), were tested. Fig. 4 shows the selected voltage vs. specific capacity profiles (Fig. 4A–C) and the specific capacity vs. cycle number (Fig. 4D–F) delivered by Li/electrolyte/SiGPAA cells upon galvanostatic cycling at different C-rates with either LiFSI or LiTFSI dissolved in the RTILs.

Table 2
Comparison of the laboratory-scale Li-metal cell (Li/electrolyte/SiGPAA) performances at 250 mA/g_{Si} (0.255 mA/cm^2) in the voltage range 0.01–2 V vs. Li^+/Li^0 (1st cycle) or 0.1–1 V vs. Li^+/Li^0 (following cycles) with different RTIL-based electrolytes.

	C.E.	Specific capacity*		Areal capacity*	Capacity retention *	
	%	mAh/g_{Si}	mAh/g	mAh/cm^2	%	%
	1st cycle	2nd cycle	2nd cycle	2nd cycle	11th cycle	53rd cycle
$Pyr_{1(201)}FSI$						
+ LiFSI	89.9	2025	813	2.1	83	74
+ LiTFSI	62.7	288	116	0.3	84	79
+ LiTFSI/VC	71.1	145	58	0.1	75	83
+ LiTFSI/FEC	12.4	122	49	0.1	61	57
$Pyr_{13}FSI$						
+ LiFSI	89.1	1652	663	1.7	83	74
+ LiTFSI	67.5	129	52	0.1	89	86
+ LiTFSI/VC	77.2	218	88	0.2	76	77
+ LiTFSI/FEC	75.6	345	139	0.4	87	85
EMIFSI						
+ LiFSI	78.0	2067	830	2.1	83	70
+ LiTFSI	83.1	1700	683	1.7	70	55
+ LiTFSI/VC	70.8	515	207	0.5	78	67
+ LiTFSI/FEC	80.1	635	255	0.6	89	89
Liquid electrolyte**	90.0	2803	1126	2.9	72	66

* lithiation, ** composition: $LiPF_6$ 1 M in EC/PC/EMC/DEC + 2 wt% VC.

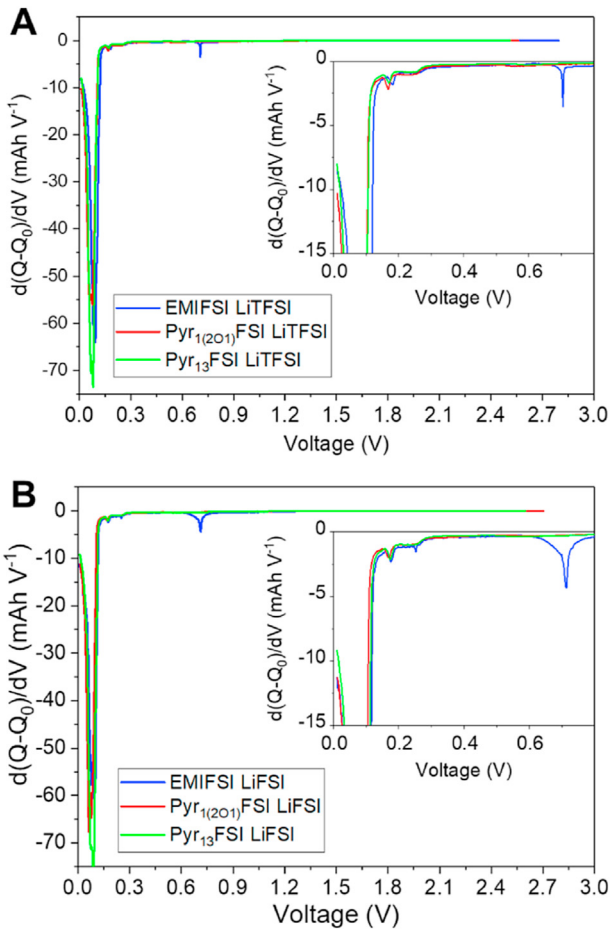

Fig. 3. Derivative dQ/dV curves corresponding to the first CC lithiation of SiGPAA (mass loading 1.03 mg/cm^2, i.e. 0.41 mg$_{Si}$/cm^2) in Li/electrolyte/SiGPAA half-cells containing (a) LiTFSI or (b) LiFSI at low current density (0.047 mA/cm^2, i.e. 115 mA/g$_{Si}$) with a cut-off voltage of 0.01 V vs. Li^+/Li^0. The insets show a magnification in the range 0–0.8 V vs. Li^+/Li^0.

The cells were operated in the voltage range 0.01–2 V (insets in Fig. 4A–C) during the first cycle, and subsequently in the range 0.1–1 V (see Fig. 4A–C) [38]. With FSI^- as the anion in both the lithium salt and the RTIL, the specific lithiation capacity delivered by the cells during the first cycle is 4494, 3778 and 3128 mAh/g$_{Si}$ (see insets in Fig. 4A–C) with Coulombic efficiency (C.E.) values of 78.0, 89.9 and 89.1% for EMIFSI, $Pyr_{1(2O1)}FSI$ and $Pyr_{13}FSI$, respectively (see Table 2). The lower C.E. obtained with EMIFSI accounts for EMI^+ decomposition at the surface of the SiGPAA electrodes.

During the following ten cycles at C/10, the delivered capacity is lower than that exhibited at the first cycle due to the reduced voltage cut-off. Under these cycling conditions, the lithiation capacity retention after 10 cycles at C/10 is about 83% for all the investigated systems utilising only FSI^- anion. In these systems, at higher C-rates, the electrochemical behaviour is relatively similar for the Pyr-based electrolytes, whereas EMIFSI systems guarantee a higher delivered capacity of ≈800 and 450 mAh/g$_{Si}$ at C/2 and 1C (2500 mA/g$_{Si}$, *viz.* 2.50 mA/cm^2), respectively. The superior performances of EMIFSI-based electrolytes can be most likely ascribed to the higher ionic conductivity and lower viscosity of the system. The cells utilising only FSI^- anion showed capacity retention of 70–75% after increasing C-rates cycling protocol (rate capability test) when the current was lowered back to C/10, thus suggesting structural stability of the SiGPAA electrode and the good SEI forming ability of the FSI^--based RTIL electrolytes, despite the absence of any further additive [18,20].

For Pyr-based electrolytes containing LiTFSI as the Li^+ ion source, the cell performance is remarkably reduced under the same cycling conditions: with $Pyr_{1(2O1)}FSI$ and $Pyr_{13}FSI$, the specific capacity delivered by the test cells cycled in the reduced voltage window is below 300 mAh/g$_{Si}$ even at low C/10 rate. For the LiTFSI-EMIFSI electrolyte, the specific lithiation capacity and C.E. of the first cycle are 3412 mAh/g$_{Si}$ and 83%, respectively. The capacity retention in the reduced voltage window is 70% after ten cycles at C/10 (see Table 2). The specific capacity delivered by the cell is below 1000 mAh/g at C/5, dropping to ≈130 mAh/g$_{Si}$ at 1C. The capacity retention at C/10 (0.255 mA/cm^2) after 52 cycles at different current densities is about 54%.

Overall, the cells assembled with the RTIL-based electrolyte formulations containing the LiFSI salt outperform their counterparts with LiTFSI salt using SiGPAA electrodes with an overall mass loading of ≈2.5 mg/cm^2, particularly with pyrrolidinium-based RTILs. In this respect, it is worth noticing that using SiGPAA electrodes with a lower mass loading, the CC cycling at 0.255 mA/cm^2 (corresponding to C/10 and~C/4 for the SiGPAA electrodes with an overall mass loading of 2.54 and 1.03 mg/cm^2, respectively) leads to a strongly improved cell performance with LiTFSI (specific capacity up to 1908 mAh/g$_{Si}$, see Fig. S5). However, the corresponding areal capacity delivered under this condition is only about 0.88 mAh/cm^2, which is less than half of that achieved at C/10 by the best cells with a SiGPAA loading of ≈2.5 mg/cm^2 in the same cut-off voltage window (see Table 2). The decreased electrode performance at increased active material loading can be linked with the expected increased electrode mechanical instability and polarisation, requiring specific additives and/or additional electrode manufacturing optimisation to be mitigated [52].

In a bid to improve the passive layer quality and cell performance in the presence of LiTFSI at higher SiGPAA mass loading (≈2.5 mg/cm^2), the addition of 3 wt% FEC or VC to the RTIL-based electrolytes was evaluated. Indeed, the use of these organic additives to RTIL-based electrolytes containing $TFSI^-$ was found to improve the cycling performance with both graphite [53,54] and Si (nanowires) [21] anodes due to their substantial influence on the composition of the SEI layer. Fig. S6 and Table 2 summarise the ambient temperature electrochemical behaviour results in lab-scale Li/electrolyte/SiGPAA cells. A slight improvement is observed with $Pyr_{13}FSI$, particularly with FEC (the specific capacity at C/10 is more than doubled compared to the pristine formulation, and the 1st cycle C.E. increased by 8%). Nonetheless, the specific capacity delivered by the cell is below 400 mAh/g$_{Si}$ at C/10. In the case of the electrolytes based on $Pyr_{1(2O1)}FSI$ and EMIFSI, the additives are detrimental both in terms of specific capacity and 1st cycle C.E. Overall, we can conclude that SEI-forming additives in the presence of RTILs containing FSI^- anion do not lead to a substantial improvement of the electrochemical performance. A similar phenomenon was observed upon the addition of VC to RTIL-based electrolytes having FSI anion in combination with graphite electrodes [55], and it might be attributed to the formation of a thicker and resistive SEI layer. In this respect, the concurrent role of the RTIL cation, additive and carbon content in the electrode are worth further investigation focused on the interface characterisation rather than the electrochemical performance, which is out of the scope of the present work.

Overall, EMIFSI is the only RTIL investigated, enabling acceptable cell performances with both LiFSI and LiTFSI, despite lower capacity retention with the latter. Therefore, to shed light on the nature of the SEI layer upon cycling, we studied the chemical composition of the surfaces of post mortem silicon electrodes collected after cycling using EMIFSI-based electrolytes with LiTFSI-

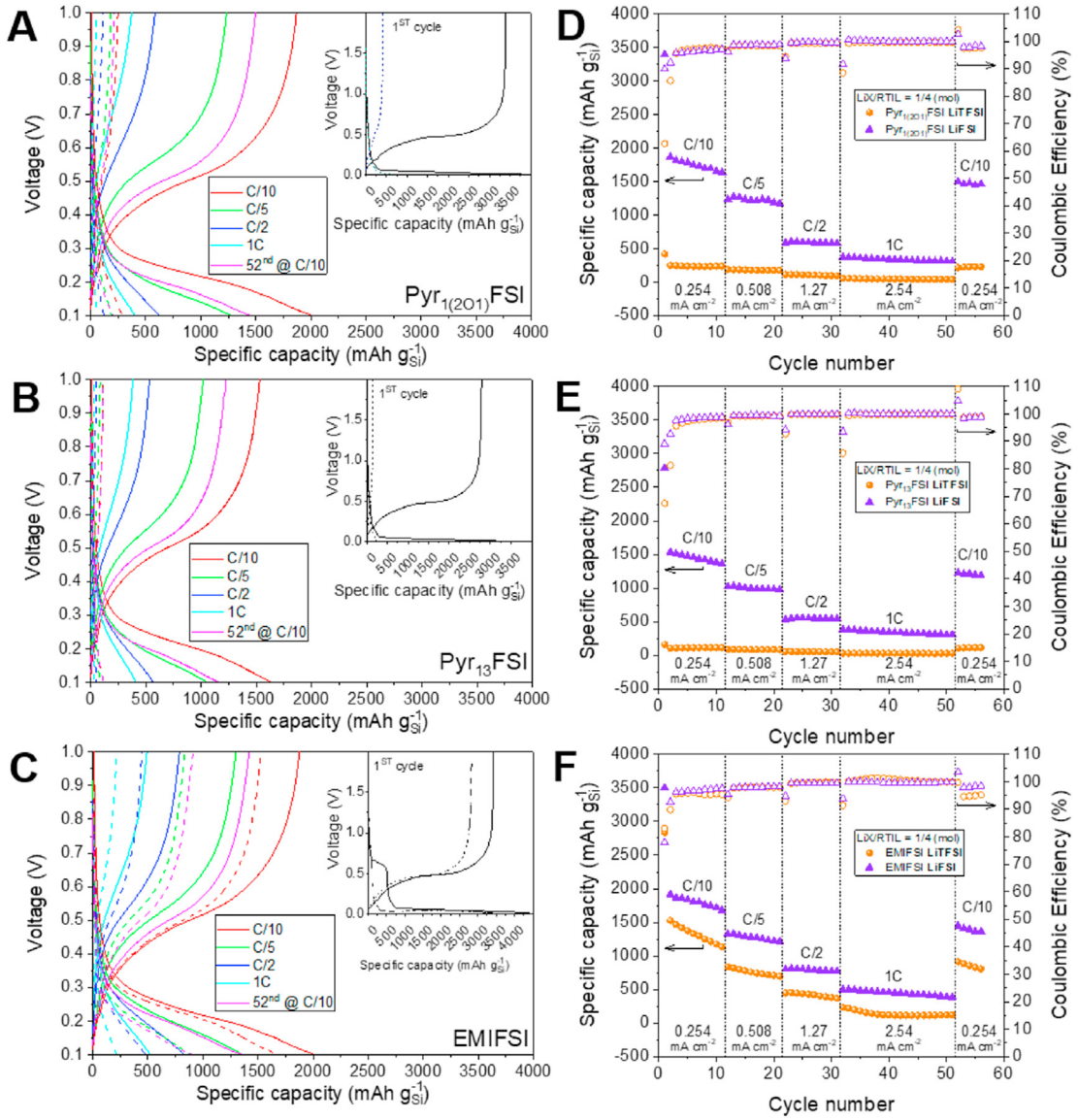

Fig. 4. Voltage vs. gravimetric specific capacity profiles during the CC cycling in the range 0.01–2 V vs. Li^+/Li^0 (1st cycle at C/10 i.e. 250 mA/g_{Si}, insets) and 0.1–1 V vs. Li^+/Li^0 (following cycles at different C-rates) of Li/electrolyte/SiGPAA half-cells (A–C) and corresponding gravimetric specific de-lithiation capacity and Coulombic efficiency vs. cycle number (D–F). The RTIL-based electrolytes contain either LiTFSI (dashed lines in A-C, orange in D-F) or LiFSI (solid lines in A-C, violet in D-F) dissolved in (A,D) $Pyr_{1(2O1)}FSI$, (B,E) $Pyr_{13}FSI$, or (C,F) EMIFSI. Open symbols = Coulombic efficiency, solid symbols = de-lithiation specific capacity. The gravimetric specific capacity is referred to the active Si content only. The SiGPAA mass loading is 2.54 mg/cm^2 (≈1.0 mg_{Si}/cm^2; maximum practical capacity ≈ 2.5 mAh/cm^2 in the range 0.1–1 V vs. Li^+/Li^0).

or LiFSI salts (Fig. S7). Two Si-based electrodes were collected from lab-scale Li-metal cells after 10 cycles at C/10 for ATR-FTIR ex situ analysis to highlight the impact of the anion on the chemical nature of the SEI. The comparison of the two ATR-FTIR spectra are shown in Fig. S7 in the supplementary data. The surface of electrodes collected post-mortem show vibrational fingerprints due to the accumulation of organic and inorganic by-products originating from the SEI components. In particular, evidence of Li_2O, Li_2CO_3, as well as organic (poly-)carbonates/(poly-)anhydrides/(poly-)esters with aliphatic groups can be observed in both cases. However, samples collected from TFSI-containing electrolytes are richer in the inorganic components, i.e. Li_2O and Li_2CO_3, compared to electrodes collected from the EMIFSI-LiFSI electrolyte. Considering the different mechanical properties of inorganic carbonates/oxides in respect to polymers, this evidence is a direct clue of a stiffer SEI layer originating from TFSI-containing electrolytes compared to the all–FSI–based one. One may speculate that a rigid SEI layer can only poorly follow the considerable volume variation of the silicon nanoparticles and likely breaks, thus exposing fresh surfaces of reduced silicon directly to the electrolyte. This mechanism can justify the accumulation of thicker and more resistive SEI layers using EMIFSI-LiTFSI in respect to the EMIFSI-LiFSI electrolyte and, therefore, the worse capacity performance. Based on the considerations above reported, the EMIFSI-based electrolytes were selected to compare galvanostatic cycling in laboratory-scale SiGPAA/electrolyte/NMC full Li-ion cells.

3.3. Laboratory-scale Li-ion cells with EMIFSI-based electrolyte

The SiGPAA/electrolyte/NMC Li-ion cells electrodes capacity balance is reported in Table 3.

Based on the estimated cell capacity (see the experimental part), the lab-scale Li-ion cells were cycled at ambient temperature and

Table 3
Laboratory-scale Li-ion cells (SiGPAA/electrolyte/NMC) design with EMIFSI-based electrolytes. M.A. = active material content considered for the calculation. Ch = charge, I.C. = irreversible capacity. The estimated cell capacity was computed as detailed in the experimental part.

	Loading (A.M.)		1st Ch capacity		1st I.C.		N/P	Estimated cell capacity
	mg/cm^2 (%)		mAh/cm^2		mAh/cm^2			mAh/cm^2
	NMC	SIGPAA	NMC	SIGPAA	NMC	SIGPAA		
LiFSI	8 (94)	1.2 (100)	1.504	2.375	0.143	0.450	1.35	0.979
LiTFSI	8 (94)	1.2 (100)	1.504	2.266	0.143	0.419	1.44	1.010

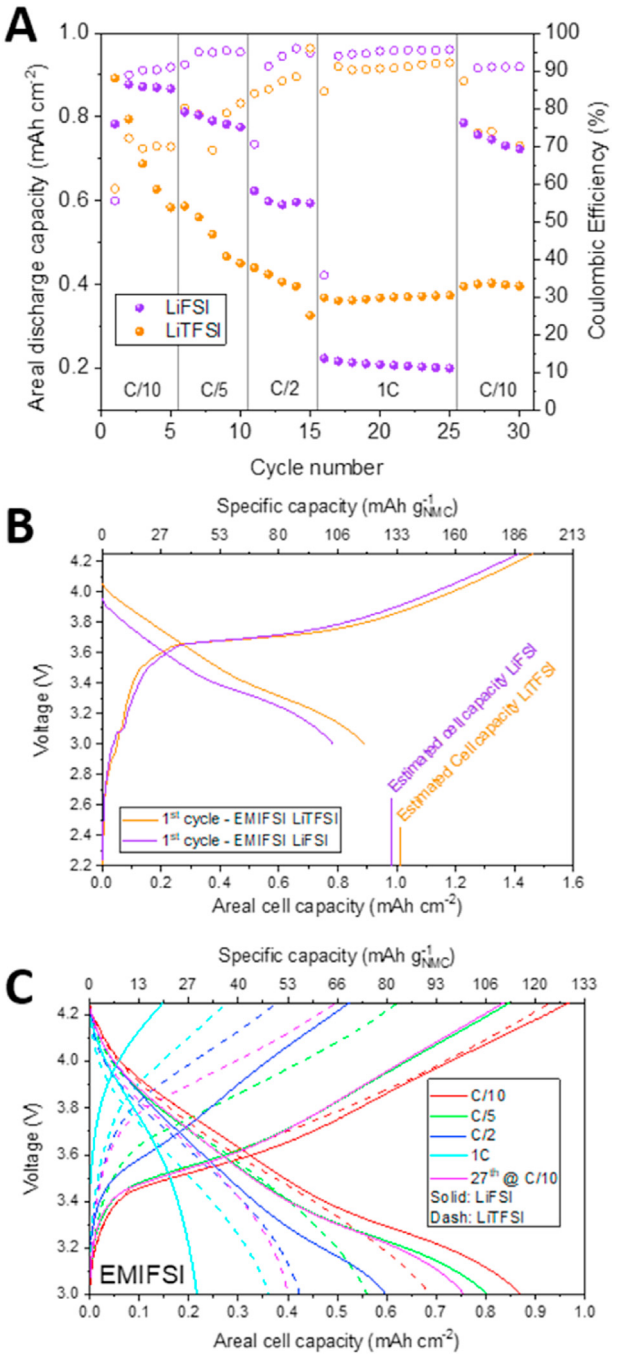

Fig. 5. – Ambient temperature electrochemical response of SiGPAA/electrolyte/NMC Li-ion cells during the CC cycling in the range 3–4.25 V vs. Li^+/Li^0 with EMIFSI-based electrolyte containing LiFSI (violet/solid lines) or LiTFSI (orange/dashed lines). The C-rate values are based on the computed estimated cell capacity in Table 3. A) Areal discharge capacity and Coulombic efficiency vs. cycle number; B) corresponding voltage profiles *vs.* the 1st cycle areal capacity. The computed estimated cell capacity is tagged on the x-axis; C) voltage profiles *vs.* areal capacity during selected cycles at different C-rates.

different C-rates from C/10 to 1C. The areal capacity *vs.* cycle number and the voltage *vs.* areal capacity plots are shown in Fig. 5.

The LiFSI-EMIFSI based cell discharge capacity is stable above 80% up to C/2, decreasing to ≈60% and ≈20% at C/2 and 1C, respectively. The cell capacity retention is ≈ 83% after 30 cycles when the current is lowered to C/10. Overall, the full FSI^--based battery cell shows better rate capability and C.E., essential for long-term cycling, with respect to the $TFSI^-$-based electrolyte. Under the same cycling condition, the LiTFSI-EMIFSI electrolyte reveals a substantial capacity decrease with increasing the C-rate and about a 50% capacity fading after only 30 cycles. The cycling response confirms the superior characteristics of the FSI^--based electrolyte formulation; it is in agreement with the Si-based Li-metal cell testing and the ATR-FTIR analysis here reported, suggesting the adoption of the formulation for advanced Li-ion cell application. Although, we did not focus on optimising the cell configuration for long-term cycling stability tests, the excellent compatibility of the proposed electrolyte, both with Si-based anodes and NMC cathodes, accounts for its attractive properties for successful adoption in advanced secondary Li-ion cells directed to electric transportation and large-scale energy storage applications.

4. Conclusions

EMIFSI, $PYR_{13}FSI$ and $PYR_{1(201)}FSI$ RTILs combined with the LiFSI and LiTFSI salts (mole fraction equal to 0.2) were used as electrolyte solutions for high-energy lithium-based battery systems with improved safety levels.

The ion transport properties of the RTIL-based electrolytes were investigated in a wide (−40/+80 °C) temperature range. The EMIFSI-based and the LiFSI-containing samples were found to be more conductive than the pyrrolidinium ones. Ionic conductivities higher than 10^{-4} S/cm are obtained at −20 °C, and values ranging from 10^{-3} to 10^{-2} S/cm are achieved at room temperature, making the proposed RTIL-based electrolytes appealing for wide range of operational temperatures. The compatibility of the proposed RTIL-based electrolytes with high energy density Si-based anodes was evaluated, evidencing the superior characteristics of the FSI^- and EMI^+ based electrolyte systems in terms of delivered capacity at various current rates and stability upon cycling. The better compatibility of the EMI-FSI based electrolyte is mainly addressed to the improved SEI forming ability of its components. The superior compatibility of the EMI-FSI based electrolyte is also confirmed in laboratory-scale Li-ion cells, coupling the Si-anode with a high energy density NMC cathode. Overall, the promising results obtained pose the EMI-FSI based electrolyte as an interesting candidate for the realisation of high energy density Li-ion batteries characterised by an elevated safety content.

Declaration of competing interest

The authors declare that they have no known competing financial interests or personal relationships that could have appeared to influence the work reported in this paper.

Data availability

Data will be made available on request.

Acknowledgements

The authors acknowledge financial support by the Si-DRIVE Project, which received funding from the EU's Horizon 2020 research and innovation (R&I) programme under GA 814464. This study was carried out within the MOST – Sustainable Mobility Center and received funding from the European Union Next-GenerationEU (PIANO NAZIONALE DI RIPRESA E RESILIENZA (PNRR) – MISSIONE 4 COMPONENTE 2, INVESTIMENTO 1.4 – D.D. 1033 17/06/2022, CN00000023). This manuscript reflects only the authors' views and opinions, neither the European Union nor the European Commission can be considered responsible for them. Part of research leading to this result has been supported by the project CALIPSOplus under the GA 730872 from the EU Framework Programme for Research and Innovation HORIZON 2020, for the beamtimes 20190616 and 20210263 at Soleil Synchrotron. SB and AP would like to thank Angelo Sarra, Nicholas Carboni and Oriele Palumbo for the fruitful discussion and Francesco Capitani and Ferenc Borondics of the SMIS beamline of Soleil Synchrotron for their help during the beamtimes.

Appendix A. Supplementary data

Supplementary data to this article can be found online at https://doi.org/10.1016/j.mtsust.2022.100299.

References

[1] R. Schmuch, R. Wagner, G. Hörpel, T. Placke, M. Winter, Performance and cost of materials for lithium-based rechargeable automotive batteries, Nat. Energy 3 (2018) 267–278, https://doi.org/10.1038/s41560-018-0107-2.
[2] Z. Yang, J. Zhang, M.C.W. Kintner-Meyer, X. Lu, D. Choi, J.P. Lemmon, J. Liu, Electrochemical energy storage for green grid, Chem. Rev. 111 (2011) 3577–3613, https://doi.org/10.1021/cr100290v.
[3] A. Masias, J. Marcicki, W.A. Paxton, Opportunities and challenges of lithium ion batteries in automotive applications, ACS Energy Lett. 6 (2021) 621–630, https://doi.org/10.1021/acsenergylett.0c02584.
[4] M. Weiss, R. Ruess, J. Kasnatscheew, Y. Levartovsky, N.R. Levy, P. Minnmann, L. Stolz, T. Waldmann, M. Wohlfahrt-Mehrens, D. Aurbach, M. Winter, Y. Ein-Eli, J. Janek, Fast charging of lithium-ion batteries: a review of materials aspects, Adv. Energy Mater. 11 (2021), 2101126, https://doi.org/10.1002/aenm.202101126.
[5] W. Chen, A review of materials and their future development trends for lithium ion battery anodes, IOP Conf. Ser. Earth Environ. Sci. 546 (2020), 022026, https://doi.org/10.1088/1755-1315/546/2/022026.
[6] J. Schwan, G. Nava, L. Mangolini, Critical barriers to the large scale commercialisation of silicon-containing batteries, Nanoscale Adv. 2 (2020) 4368–4389, https://doi.org/10.1039/D0NA00589D.
[7] M. Salah, P. Murphy, C. Hall, C. Francis, R. Kerr, M. Fabretto, Pure silicon thin-film anodes for lithium-ion batteries: a review, J. Power Sources 414 (2019) 48–67, https://doi.org/10.1016/j.jpowsour.2018.12.068.
[8] K. Feng, M. Li, W. Liu, A.G. Kashkooli, X. Xiao, M. Cai, Z. Chen, Silicon-based anodes for lithium-ion batteries: from fundamentals to practical applications, Small 14 (2018), 1702737, https://doi.org/10.1002/smll.201702737.
[9] E. Pollak, G. Salitra, V. Baranchugov, D. Aurbach, In situ conductivity, impedance spectroscopy, and ex situ Raman spectra of amorphous silicon during the insertion/extraction of lithium, J. Phys. Chem. C 111 (2007) 11437–11444, https://doi.org/10.1021/jp0729563.
[10] F. Dou, L. Shi, G. Chen, D. Zhang, Silicon/carbon composite anode materials for lithium-ion batteries, Electrochem. Energ. Rev. 2 (2019) 149–198, https://doi.org/10.1007/s41918-018-00028-w.
[11] Q. Shi, J. Zhou, S. Ullah, X. Yang, K. Tokarska, B. Trzebicka, H.Q. Ta, M.H. Rümmeli, A review of recent developments in Si/C composite materials for Li-ion batteries, Energy Storage Mater. 34 (2021) 735–754, https://doi.org/10.1016/j.ensm.2020.10.026.
[12] X. Zuo, J. Zhu, P. Müller-Buschbaum, Y.-J. Cheng, Silicon based lithium-ion battery anodes: a chronicle perspective review, Nano Energy 31 (2017) 113–143, https://doi.org/10.1016/j.nanoen.2016.11.013.
[13] X. Zhao, V.-P. Lehto, Challenges and prospects of nanosized silicon anodes in lithium-ion batteries, Nanotechnology 32 (2020), 042002, https://doi.org/10.1088/1361-6528/abb850.
[14] J. Wu, Y. Cao, H. Zhao, J. Mao, Z. Guo, The critical role of carbon in marrying silicon and graphite anodes for high-energy lithium-ion batteries, Carbon Energy 1 (2019) 57–76, https://doi.org/10.1002/cey2.2.
[15] L. Lavagna, G. Meligrana, C. Gerbaldi, A. Tagliaferro, M. Bartoli, Graphene and lithium-based battery electrodes: a review of recent literature, Energies 13 (2020) 4867, https://doi.org/10.3390/en13184867.
[16] G.G. Eshetu, E. Figgemeier, Confronting the challenges of next-generation silicon anode-based lithium-ion batteries: role of designer electrolyte additives and polymeric binders, ChemSusChem 12 (2019) 2515–2539, https://doi.org/10.1002/cssc.201900209.
[17] Z. Xu, J. Yang, H. Li, Y. Nuli, J. Wang, Electrolytes for advanced lithium ion batteries using silicon-based anodes, J. Mater. Chem. A. 7 (2019) 9432–9446, https://doi.org/10.1039/C9TA01876J.
[18] D.M. Piper, T. Evans, K. Leung, T. Watkins, J. Olson, S.C. Kim, S.S. Han, V. Bhat, K.H. Oh, D.A. Buttry, S.-H. Lee, Stable silicon-ionic liquid interface for next-generation lithium-ion batteries, Nat. Commun. 6 (2015) 6230, https://doi.org/10.1038/ncomms7230.
[19] N. Sanchez-Ramirez, B.D. Assresahegn, R.M. Torresi, D. Bélanger, Producing high-performing silicon anodes by tailoring ionic liquids as electrolytes, Energy Storage Mater. 25 (2020) 477–486, https://doi.org/10.1016/j.ensm.2019.09.035.
[20] G.-T. Kim, T. Kennedy, M. Brandon, H. Geaney, K.M. Ryan, S. Passerini, G.B. Appetecchi, Behavior of germanium and silicon nanowire anodes with ionic liquid electrolytes, ACS Nano 11 (2017) 5933–5943, https://doi.org/10.1021/acsnano.7b01705.
[21] K. Stokes, T. Kennedy, G.-T. Kim, H. Geaney, D. Storan, F. Laffir, G.B. Appetecchi, S. Passerini, K.M. Ryan, Influence of carbonate-based additives on the electrochemical performance of Si NW anodes cycled in an ionic liquid electrolyte, Nano Lett. 20 (2020) 7011–7019, https://doi.org/10.1021/acs.nanolett.0c01774.
[22] G.B. Appetecchi, M. Montanino, S. Passerini, Ionic liquid-based electrolytes for high energy, safer lithium batteries, in: A.E. Visser, N.J. Bridges, R.D. Rogers (Eds.), Ionic Liquids: Science and Applications, American Chemical Society, Washington, DC, 2012, pp. 67–128, https://doi.org/10.1021/bk-2012-1117.ch004.
[23] N. Plylahan, M. Kerner, D.-H. Lim, A. Matic, P. Johansson, Ionic liquid and hybrid ionic liquid/organic electrolytes for high temperature lithium-ion battery application, Electrochim. Acta 216 (2016) 24–34, https://doi.org/10.1016/j.electacta.2016.08.025.
[24] A. Balducci, Ionic liquids in lithium-ion batteries, Top. Curr. Chem. Z 375 (2017) 20, https://doi.org/10.1007/s41061-017-0109-8.
[25] M. Watanabe, M.L. Thomas, S. Zhang, K. Ueno, T. Yasuda, K. Dokko, Application of ionic liquids to energy storage and conversion materials and devices, Chem. Rev. 117 (2017) 7190–7239, https://doi.org/10.1021/acs.chemrev.6b00504.
[26] R. Kerr, D. Mazouzi, M. Eftekharnia, B. Lestriez, N. Dupré, M. Forsyth, D. Guyomard, P.C. Howlett, High-capacity retention of Si anodes using a mixed lithium/phosphonium bis(fluorosulfonyl)imide ionic liquid electrolyte, ACS Energy Lett. 2 (2017) 1804–1809, https://doi.org/10.1021/acsenergylett.7b00403.
[27] K. Yamaguchi, Y. Domi, H. Usui, M. Shimizu, K. Matsumoto, T. Nokami, T. Itoh, H. Sakaguchi, Influence of the structure of the anion in an ionic liquid electrolyte on the electrochemical performance of a silicon negative electrode for a lithium-ion battery, J. Power Sources 338 (2017) 103–107, https://doi.org/10.1016/j.jpowsour.2016.10.111.
[28] H. Shobukawa, J. Shin, J. Alvarado, C.S. Rustomji, Y.S. Meng, Electrochemical reaction and surface chemistry for performance enhancement of a Si composite anode using a bis(fluorosulfonyl)imide-based ionic liquid, J. Mater. Chem. A. 4 (2016) 15117–15125, https://doi.org/10.1039/C6TA06447G.
[29] X. Wang, M. Salari, D. Jiang, J. Chapman Varela, B. Anasori, D.J. Wesolowski, S. Dai, M.W. Grinstaff, Y. Gogotsi, Electrode material–ionic liquid coupling for electrochemical energy storage, Nat. Rev. Mater. 5 (2020) 787–808, https://doi.org/10.1038/s41578-020-0218-9.
[30] H. Zhang, W. Feng, J. Nie, Z. Zhou, Recent progresses on electrolytes of fluorosulfonimide anions for improving the performances of rechargeable Li and Li-ion battery, J. Fluor. Chem. 174 (2015) 49–61, https://doi.org/10.1016/j.jfluchem.2014.07.028.
[31] M. Kerner, N. Plylahan, J. Scheers, P. Johansson, Thermal stability and decomposition of lithium bis(fluorosulfonyl)imide (LiFSI) salts, RSC Adv. 6 (2016) 23327–23334, https://doi.org/10.1039/C5RA25048J.
[32] A. Mauger, C.M. Julien, A. Paolella, M. Armand, K. Zaghib, A comprehensive review of lithium salts and beyond for rechargeable batteries: progress and perspectives, Mater. Sci. Eng. R Rep. 134 (2018) 1–21, https://doi.org/10.1016/j.mser.2018.07.001.
[33] J. Huang, A.F. Hollenkamp, Thermal behavior of ionic liquids containing the FSI anion and the Li^+ cation, J. Phys. Chem. C 114 (2010) 21840–21847, https://doi.org/10.1021/jp107740p.
[34] E. Simonetti, M. De Francesco, M. Bellusci, G.-T. Kim, F. Wu, S. Passerini, G.B. Appetecchi, A more sustainable and cheaper one-pot route for the synthesis of hydrophobic ionic liquids for electrolyte applications, ChemSusChem 12 (2019) 4946–4952, https://doi.org/10.1002/cssc.201902054.
[35] M. Kerner, N. Plylahan, J. Scheers, P. Johansson, Ionic liquid based lithium battery electrolytes: fundamental benefits of utilising both TFSI and FSI anions? Phys. Chem. Chem. Phys. 17 (2015) 19569–19581, https://doi.org/10.1039/C5CP01891A.

[36] S. Brutti, E. Simonetti, M. De Francesco, A. Sarra, A. Paolone, O. Palumbo, S. Fantini, R. Lin, A. Falgayrat, H. Choi, others, Ionic liquid electrolytes for high-voltage, lithium-ion batteries, J. Power Sources 479 (2020), 228791, https://doi.org/10.1016/j.jpowsour.2020.228791.
[37] E. Greco, G. Nava, R. Fathi, F. Fumagalli, A.E.D. Rio-Castillo, A. Ansaldo, S. Monaco, F. Bonaccorso, V. Pellegrini, F.D. Fonzo, Few-layer graphene improves silicon performance in Li-ion battery anodes, J. Mater. Chem. A. 5 (2017) 19306–19315, https://doi.org/10.1039/C7TA05395A.
[38] S. Palumbo, L. Silvestri, A. Ansaldo, R. Brescia, F. Bonaccorso, V. Pellegrini, Silicon few-layer graphene nanocomposite as high-capacity and high-rate anode in lithium-ion batteries, ACS Appl. Energy Mater. 2 (2019) 1793–1802, https://doi.org/10.1021/acsaem.8b01927.
[39] M. Falco, S. Palumbo, G. Lingua, L. Silvestri, M. Winter, R. Lin, V. Pellegrini, F. Bonaccorso, J.R. Nair, C. Gerbaldi, A bilayer polymer electrolyte encompassing pyrrolidinium-based RTIL for binder-free silicon few-layer graphene nanocomposite anodes for Li-ion battery, Electrochem. Commun. 118 (2020), 106807, https://doi.org/10.1016/j.elecom.2020.106807.
[40] Y. Domi, H. Usui, K. Yamaguchi, S. Yodoya, H. Sakaguchi, Silicon-based anodes with long cycle life for lithium-ion batteries achieved by significant suppression of their volume expansion in ionic-liquid electrolyte, ACS Appl. Mater. Interfaces 11 (2019) 2950–2960, https://doi.org/10.1021/acsami.8b17123.
[41] D.T. Rogstad, M.-A. Einarsrud, A.M. Svensson, Evaluation of selected ionic liquids as electrolytes for silicon anodes in Li-ion batteries, J. Electrochem. Soc. 168 (2021), 110506, https://doi.org/10.1149/1945-7111/ac330f.
[42] A.D.R. Castillo, V. Pellegrini, A. Ansaldo, F. Ricciardella, H. Sun, L. Marasco, J. Buha, Z. Dang, L. Gagliani, E. Lago, others, High-yield production of 2D crystals by wet-jet milling, Mater. Horiz. 5 (2018) 890–904, https://doi.org/10.1039/C8MH00487K.
[43] W.A. Henderson, S. Passerini, Phase behavior of ionic Liquid–LiX mixtures: pyrrolidinium cations and TFSI- anions, Chem. Mater. 16 (2004) 2881–2885, https://doi.org/10.1021/cm049942j.
[44] C. Bongiorno, G. Mannino, U. D'Alessio, F. Monforte, G.G. Condorelli, C. Spinella, A. La Magna, S. Brutti, On the redox activity of the solid electrolyte interphase in the reduction/oxidation of silicon nanoparticles in secondary lithium batteries, Energy Technol. 10 (2022), 2100791, https://doi.org/10.1002/ente.202100791.
[45] I.D. Raistrick, D.R. Franceschetti, J.R. Macdonald, Theory, in: Impedance Spectroscopy, John Wiley & Sons, 2005, pp. 27–128, https://doi.org/10.1002/0471716243.ch2.
[46] G.-T. Kim, G.B. Appetecchi, M. Montanino, F. Alessandrini, S. Passerini, (Invited) long-term cyclability of lithium metal electrodes in ionic liquid-based electrolytes at room temperature, ECS Trans. 25 (2010) 127, https://doi.org/10.1149/1.3393847.
[47] B.A. Boukamp, A package for impedance/admittance data analysis, Solid State Ionics 18–19 (1986) 136–140, https://doi.org/10.1016/0167-2738(86)90100-1.
[48] B.A. Boukamp, A Nonlinear Least Squares Fit procedure for analysis of immittance data of electrochemical systems, Solid State Ionics 20 (1986) 31–44, https://doi.org/10.1016/0167-2738(86)90031-7.
[49] G.B. Appetecchi, M. Montanino, M. Carewska, M. Moreno, F. Alessandrini, S. Passerini, Chemical–physical properties of bis(perfluoroalkylsulfonyl) imide-based ionic liquids, Electrochim. Acta 56 (2011) 1300–1307, https://doi.org/10.1016/j.electacta.2010.10.023.
[50] W.A. Henderson, J. Victor G. Young, D.M. Fox, H.C.D. Long, P.C. Trulove, Alkyl vs. alkoxy chains on ionic liquid cations, Chem. Commun. (2006) 3708–3710, https://doi.org/10.1039/B606381K.
[51] M.T. McDowell, S.W. Lee, W.D. Nix, Y. Cui, 25th anniversary article: understanding the lithiation of silicon and other alloying anodes for lithium-ion batteries, Adv. Mater. 25 (2013) 4966–4985, https://doi.org/10.1002/adma.201301795.
[52] W. Ji, H. Qu, X. Zhang, D. Zheng, D. Qu, Electrode architecture design to promote charge-transport kinetics in high-loading and high-energy lithium-based batteries, Small Methods 5 (2021), 2100518, https://doi.org/10.1002/smtd.202100518.
[53] S.F. Lux, M. Schmuck, G.B. Appetecchi, S. Passerini, M. Winter, A. Balducci, Lithium insertion in graphite from ternary ionic liquid–lithium salt electrolytes: II. Evaluation of specific capacity and cycling efficiency and stability at room temperature, J. Power Sources 192 (2009) 606–611, https://doi.org/10.1016/j.jpowsour.2009.02.066.
[54] I.A. Profatilova, N.-S. Choi, S.W. Roh, S.S. Kim, Electrochemical and thermal properties of graphite electrodes with imidazolium- and piperidinium-based ionic liquids, J. Power Sources 192 (2009) 636–643, https://doi.org/10.1016/j.jpowsour.2009.03.041.
[55] T. Sugimoto, Y. Atsumi, N. Handa, M. Yamagata, M. Kono, M. Kikuta, E. Ishiko, M. Ishikawa, Effects of organic additives on lithium insertion/extraction for graphite electrode in ionic liquid electrolytes based on bis(fluorosulfonyl) imide, Electrochemistry 77 (2009) 696–698, https://doi.org/10.5796/electrochemistry.77.696.